Electric Field-driven Jet Printing of Flexible Transparent Conductive Films

Fulai Cao, Yanpu Chao, Jiaping Chen, Xianhao Ma, Xiaobo Zhao, and Yizhuo Shi

Abstract—**The application of indium tin oxide (ITO) materials in flexible electronic devices is hindered by their brittleness, high cost, and toxicity. Transparent metal mesh films, such as those incorporating nano-silver grids, offer significant advantages and represent a promising alternative to ITO materials. However, current printing technologies are constrained by the nozzle diameter, and it is thus challenging to achieve patterns with line widths smaller than the nozzle size. Moreover, printing high-viscosity, high-silver-content nano-silver inks remains problematic. To overcome these issues, in this study, a novel method based on electric field-driven jet printing is proposed for fabricating flexible transparent conductive films with metal mesh structures. The fundamental principles behind this process are analyzed, and the cone-jet formation process is experimentally observed. The range of processing parameters suitable for printing nano-silver ink on polyethylene terephthalate substrates is determined, enabling the controlled printing of various line patterns, including stretchable structures. A 40 × 40-mm^2 metal mesh transparent conductive film is fabricated under optimized conditions, exhibiting a high optical transmittance (83.36%), low sheet resistance (2.08 Ω·sq^{-1}), and high figure of merit (951). This method offers a novel approach for the low-cost manufacturing of flexible, high-performance electronic devices.**

Index Terms—**Electric field-driven jet printing, Flexible electronics, Metal-grid electrodes, Nano-silver ink, Transparent conductive film**

I. Introduction

Flexible transparent conductive films demonstrate a unique combination of good optical transparency, high electrical conductivity, and excellent mechanical properties, including ductility, flexibility, and bending resistance [1, 2]. Consequently, they offer broad range of application prospects in optoelectronic fields [3], including touch screens [4], displays (in particular, flexible and foldable displays) [5], organic light-emitting diodes [6], liquid-crystal displays, smart window [7], and wearable smart devices [8]. At present, indium tin oxide (ITO) is currently the standard transparent electrode material in commercial applications because of its excellent conductivity and optical transparency [9]. Nevertheless, its widespread use in flexible electronics is hindered by several drawbacks, including its brittle nature, susceptibility to fracture, and elevated production costs. Additionally, the limited availability of indium and the requirement for high-temperature fabrication further constrain its practicality [10]. Consequently, development of alternative flexible transparent conductive materials that not only demonstrate excellent optoelectronic properties, but also exhibit uniform sheet resistance, good mechanical flexibility, stability, and cost-effectiveness, is urgently required.

In recent years, considerable interest has emerged in the field of flexible electronics regarding various alternative materials. These include carbon-based options like graphene and carbon nanotubes (CNTs), conductive polymers such as poly(3,4-ethylenedioxythiophene) (PEDOT), and metal-based components, including thin metal films, metallic grids, and nanowires. Among these, conductive polymer films (e.g., PEDOT), metal-grid transparent conductive films, metal nanowires (e.g., silver nanowires), CNTs, and graphene are considered ideal alternatives to replace ITO as next-generation transparent conductive materials [11]. Although CNTs and graphene exhibit good conductivity and transparency, their fabrication processes typically involve complex techniques, such as magnetron sputtering and vacuum deposition, resulting in high production costs and therefore limiting their practical applications [12]. Conductive polymer films, while being easily prepared via solution-based methods, such as spin coating and printing, often exhibit a higher sheet resistance than ITO under similar conditions [13]. By contrast, metal-grid transparent films, in particular, silver nanowire grids, not only match the transmittance and conductivity of ITO, but also offer superior flexibility, lower cost, and greater customizability. Therefore, they are considered among the most promising candidates for next-generation transparent electrodes from both academic and industrial perspectives [14].

To date, various methods, including photolithography, nanoimprinting, laser direct writing, inkjet printing, aerosol jet printing, and electrohydrodynamic (EHD) jet printing [15]

Manuscript received September 24, 2024; revised April 2, 2025.

This work was supported in part by the Science and Technology Tackling Project of Henan Province (Grant Nos. 242102220073, 242102231054); Key Scientific Research Project of Higher Education Institutions of Henan Province (Grant No. 25B460011); National Innovation and Entrepreneurship Training Program for College Students (Grant No. 202410480001).

Fulai Cao is a lecturer of School of Mechatronics Engineering, Xuchang University, Xuchang 4561000, China. (Corresponding author to provide phone:86-0374-2996779; e-mail: cfulai@163.com).

Yanpu Chao is a professor of School of Mechatronics Engineering, Xuchang University, Xuchang 4561000, China. (e-mail: chaoyanpu@163.com).

Jiaping Chen is a deputy chief engineer at the Beijing Institute of Spacecraft Environmental Engineering, Beijing 100094, China. (e-mail: chenjiaping2004@163.com).

Xianhao Ma is an undergraduate student of School of Mechatronics Engineering, Xuchang University, Xuchang 4561000, China. (e-mail: mxhao2004@163.com).

Xiaobo Zhao is an undergraduate student of School of Mechatronics Engineering, Xuchang University, Xuchang 4561000, China. (e-mail: 15839388945@163.com).

Yizhuo Shi is an undergraduate student of School of Mechatronics Engineering, Xuchang University, Xuchang 4561000, China. (e-mail: cxcykm@163.com).

have been proposed for fabricating silver-grid transparent electrodes. However, each of these techniques is associated with limitations. For instance, while photolithography is widely used for metal-grid transparent electrodes, it involves long production cycles, high costs, and difficulties in fabricating large-area electrodes, especially on flexible substrates [16]. Conversely, nanoimprinting offers high resolution, uniformity, and efficiency, but faces challenges in the large-area fabrication of electrodes on rigid substrates due to several issues, such as pattern deformation and detachment, caused by the excessive contact between the template and the imprint pattern [17]. Moreover, producing printing masters is not only time-consuming, but also expensive. Femtosecond-laser direct writing requires expensive lasers, and the obtained silver wires often acquire rough edges, resulting in low material utilization and significant waste [18]. Inkjet printing, whether thermal or piezoelectric, is limited by a poor resolution (typically, line widths are greater than 20 μm) and low material viscosity (generally below 30 mPa·s), which make it unsuitable for printing high-viscosity, high-silver-content nano-inks. Although aerosol jet printing achieves a higher precision (with a resolution as high as 5 μm), it remains limited by the material viscosity, which generally cannot exceed 1000 mPa·s, thus hindering its use with high-viscosity, silver-rich inks [19]. Moreover, the equipment cost for aerosol jet printing is high.

Noteworthy, EHD jet printing employs electric field forces to draw liquid from the tip of a Taylor cone, enabling high-resolution printing of high-viscosity silver inks with a higher solid content than traditional inkjet and aerosol jet printing. However, this method requires a grounded counter-electrode, and the applied voltage must increase proportionally with the layer height of the printed object. Typically, the distance between the conductive nozzle and the substrate must be kept below 5 mm, which limits its applicability in large-scale objects and hybrid micro–macro structures [20]. Furthermore, residual charges often cause short circuits and discharge events, which significantly restrict the printing range and stability when fabricating silver-grid transparent electrodes [21, 22].

To address these issues, the current study proposes a novel method that employs an electric field to fabricate large-area metal-grid transparent conductive films. Experiments were conducted to deposit nano-silver inks and investigate the effects of the applied voltage, air pressure, and printing speed on the obtained line width and morphology. A 40 × 40-mm^2 grid transparent conductive film was successfully fabricated, which exhibits a high optical transmittance in the visible spectrum and a low sheet resistance. This approach provides a promising solution for achieving high-performance, large-area, and cost-effective production of transparent conductive films.

II. Materials and Methods

A. Basic Principle of Electric Field-driven Jet Printing

The electric field-driven jet printing system comprises multiple essential functional components, including a motion control system, a backpressure regulation unit, a material

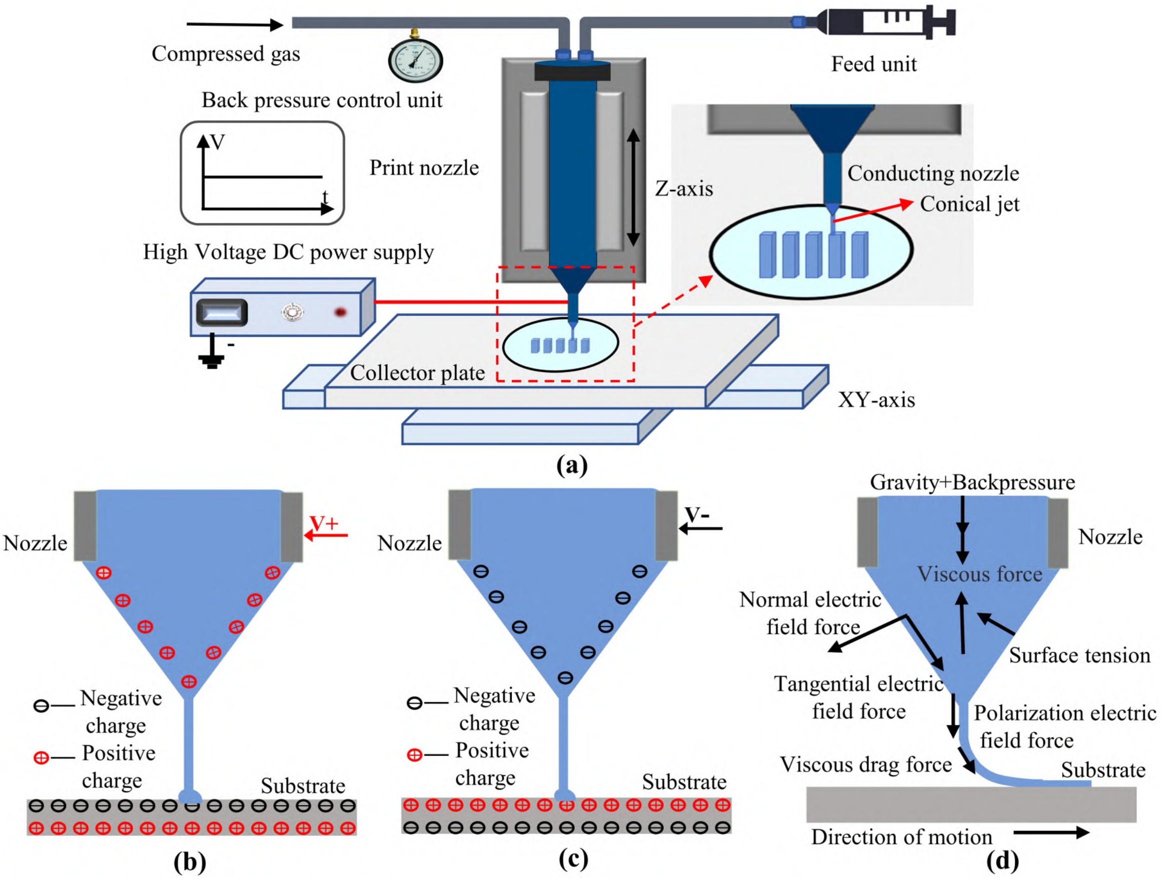

Fig. 1 Electric field-driven jet printing: (a) overall structure of the system; (b) electric field state under application of a positive voltage; (c) electric field state under application of a negative voltage; (d) force analysis of the printing process.

supply mechanism, a substrate, a high-voltage power source, and a printing nozzle. Figure 1(a) presents a schematic diagram of this three-dimensional (3D) jet-deposition printing system. The metallic printing nozzle, mounted on a Z-axis motion platform, is connected to a high-voltage DC power source. Its upper section is linked to both the material supply unit and the backpressure regulation system. While the material supply unit continuously replenishes the printing material, the backpressure control system precisely manages the meniscus shape at the nozzle tip and regulates material flow.

Electric field-driven jet printing is an advanced micro-jet deposition technique that leverages electrostatic induction and the principles of EHD. Traditional EHD jet printing relies on a conductive nozzle (serving as the first electrode) and a conductive substrate (acting as the second electrode). In contrast, the electric field-driven approach eliminates the need for a grounded counter-electrode by utilizing only a conductive nozzle connected to a high-voltage pulsed power supply. The required electric field for jetting is generated through electrostatic induction [23]. When a positive high voltage is applied to the conductive nozzle, it induces an electrostatic interaction with the substrate, redistributing charges—negative charges accumulate on the top surface while positive charges migrate downward, as illustrated in Figure 1(b). Conversely, applying a negative high voltage to the nozzle leads to the opposite charge redistribution. This continuous electrostatic influence directs the printing material onto the designated substrate, as shown in Figure 1(c).

During operation, the slurry within the nozzle initially exits due to gravity and air pressure. The interplay of gravity, air pressure, and surface tension stabilizes the meniscus at the nozzle tip. Upon connection to the high-voltage DC power source, an electric field forms between the nozzle and the substrate, inducing polarization in the liquid droplets at the nozzle tip. The combined effects of electric field forces (including tangential, normal, and polarization forces), surface tension, viscosity, gravity, and air pressure cause the droplets to elongate, forming a Taylor cone, as depicted in Figure 1(d). When the electric field force surpasses the surface tension and viscosity of the liquid, a fine jet emerges from the Taylor cone's apex, often exhibiting a diameter one to two orders of magnitude smaller than the nozzle opening. Upon contact with the collection plate, the jet undergoes further narrowing due to viscous drag. After depositing the initial layer, the Z-axis platform elevates by a single layer height, allowing the formation of a new electric field between the conductive nozzle and the previously deposited structure. This layer-by-layer approach eliminates the necessity to increase voltage as the printed object grows in height, facilitating the precise fabrication of high-resolution 3D structures.

TABLE I

PERFORMANCE PARAMETERS OF THE NANO-SILVER INK

Parameter	Value
Viscosity (mPa·s)	≥1500 (25 °C)
Silver mass fraction (%)	≥80
Density (g·cm^{-3})	2.3
Nano-silver particle size (nm)	200–300
Resistivity (mΩ·μm)	200
Adhesion (B)	4 (after sintering at 130 °C for 30 min, tested via the 3M tape cross-hatch method)

B. Materials

The printing experiments utilized a stainless-steel needle nozzle featuring an inner diameter of 300 μm. As the printing material, a high-viscosity nano-silver ink with an elevated silver concentration was selected. Table I provides a summary of the ink's primary performance characteristics.

III. EXPERIMENTAL RESULTS AND DISCUSSION

A. Formation and Evolution of Cone Jet and Silver Wire

The printing process parameters are as follows: The diameter of nozzle was 300 μm, the gas pressure was set to 130 kPa, the distance between the nozzle and polyethylene terephthalate (PET) substrate was set to 0.3 mm, and the applied DC voltage was set to 1.2 kV. Fig. 2(a) illustrates that without the application of a high voltage, backpressure and gravity cause the silver nanoparticle ink to form a stable

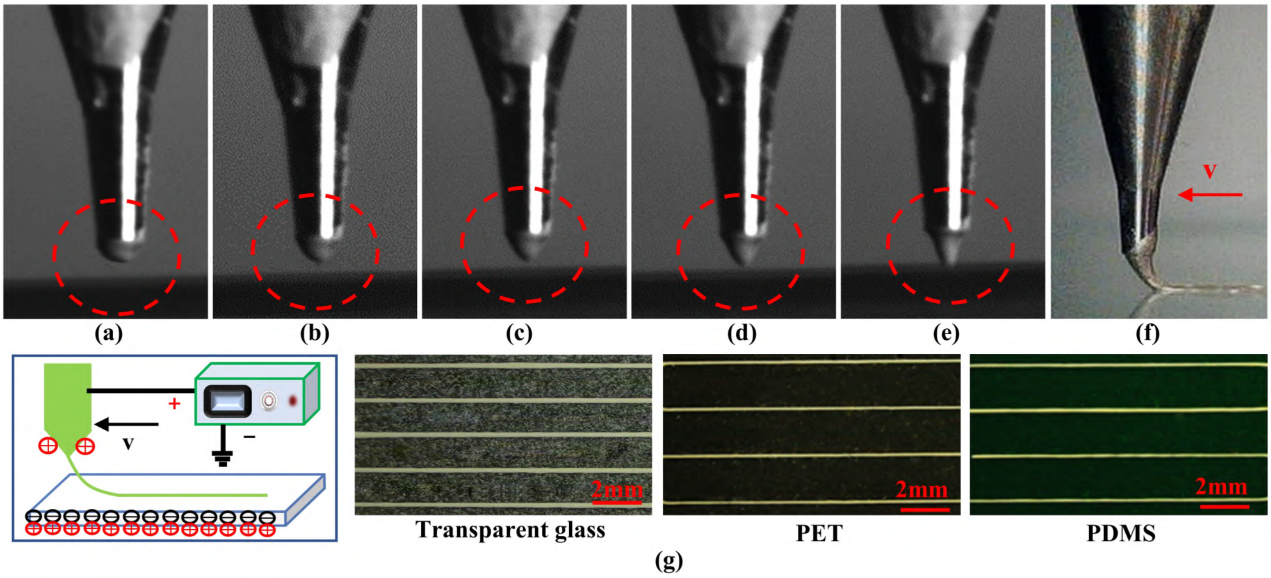

Fig. 2 Formation of the cone jet and silver line: (a)–(e) formation of the cone jet; (f) formation of the silver line; (g) silver wires deposited on different substrates.

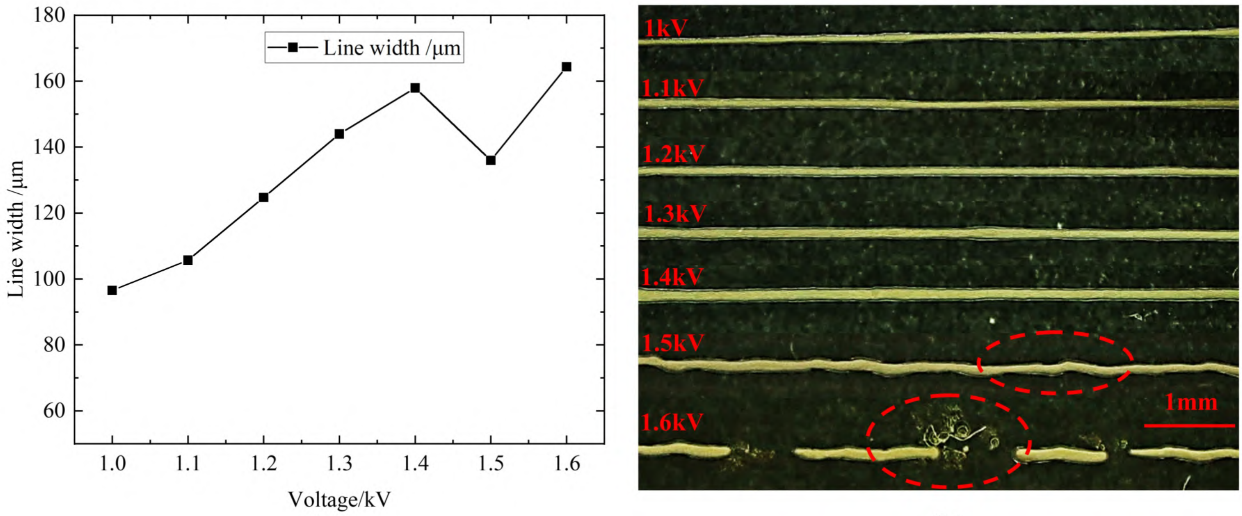

(a) (b)

Fig. 3 Effect of the applied voltage on the line width and shape of the printed silver wires: (a) line width; (b) line shape.

meniscus at the nozzle tip. When a high voltage is applied, as shown in Fig. 2(b), the meniscus becomes polarized due to electrostatic induction, leading to a stretching deformation. As the polarization voltage increases, the meniscus extends due to the combined effects of electric field forces, surface tension, viscosity, and backpressure, eventually developing into a Taylor cone, as shown in Fig. 2(c) and (d). Once the electric field force surpasses the ink's surface tension, a stable and continuous cone jet emerges from the Taylor cone's tip, with the jet diameter being one to two orders of magnitude smaller than the nozzle diameter, as illustrated in Fig. 2(e). Combined with the movement of the working platform, this enables high-resolution deposition of silver wires on the substrate, as demonstrated in Fig. 2(f). Fig. 2(g) presents the deposition results on transparent glass, PET, and polydimethylsiloxane substrates, showing silver wires with uniform line widths. These results confirm the feasibility and stability of the proposed printing method on non-conductive substrates.

B. Printing Process of Silver-Nanoparticle Ink on PET

PET is an excellent flexible substrate material extensively used in the flexible transparent electronics industry due to its remarkable optical properties, weather resistance, flexibility, and dimensional stability. Moreover, PET is non-toxic, lightweight, and inexpensive. Conductive structures printed on PET substrates are suitable for applications in flexible displays, transparent heating elements, electromagnetic shielding, and wearable electronics. Therefore, determination of the most suitable range of processing parameters for printing flexible electronic devices on PET substrates holds considerable research significance.

(1) Effect of the Printing Voltage

Printing voltage is a critical process parameter that directly influences the resolution and morphology of printed materials. A high DC voltage applied to the nozzle generates an electric field between the nozzle and the substrate. By adjusting the voltage, the electric field strength can be controlled, which thus affects the morphology of the obtained silver wire. In this experiment, the printing results were examined at voltages of 1, 1.1, 1.2, 1.3, 1.4, 1.5, and 1.6 kV, respectively, while maintaining the other parameters constant, namely a printing height of 300 μm, a gas pressure of 130 kPa, a printing speed of F50, and a nozzle diameter of 300 μm.

Figure 3(a) presents the correlation between the applied voltage and the line width of the printed silver wires. The findings indicate that, irrespective of voltage magnitude, the line width remains narrower than the nozzle diameter, with the smallest recorded value measuring 32% of the nozzle diameter. Generally, as the printing voltage rises, the line width expands, though a slight decrease is observed at 1.5 kV. Fig. 3(b) shows morphological changes in the silver wires printed at different voltages. At 1 kV, the line width is uneven; at 1.1 kV, the line width uniformity improves. Within the voltage range from 1.2 to 1.4 kV, the printed silver wires exhibit the best continuity and uniformity. However, at 1.5 kV, the wire develops wavy distortions, which reduce its uniformity. At 1.6 kV, wire breakage occurs, accompanied by the formation of scattered silver ink droplets near the fracture points.

These phenomena are primarily attributed to the variations in electric field intensity induced by different applied voltages. At voltages between 1 and 1.1 kV, although Taylor cones and jets are formed, the induced electric field intensity is insufficient, resulting in unstable jets and irregular line widths. With the increase in the voltage to 1.2–1.4 kV, the electric field intensity reaches an optimal range, resulting in stable Taylor cones and jets. This stability leads to the formation of continuous, uniform, and well-defined silver wires. Furthermore, higher voltages generate greater electric forces, increasing the ejection rate of silver ink and causing a corresponding increase in line width. However, at voltages between 1.5 and 1.6 kV, the excessive electric field intensity leads to jet oscillations and wire distortions. Furthermore, the elevated electric field strength causes splashing during ink deposition, increasing edge roughness and resulting in wire breakage at 1.6 kV.

(2) Effect of the Printing Pressure

The printing pressure directly affects the material feed rate; and stable, uniform printing is only achievable when the material feed rate matches the printing speed. To thoroughly investigate the effect of the printing pressure on the

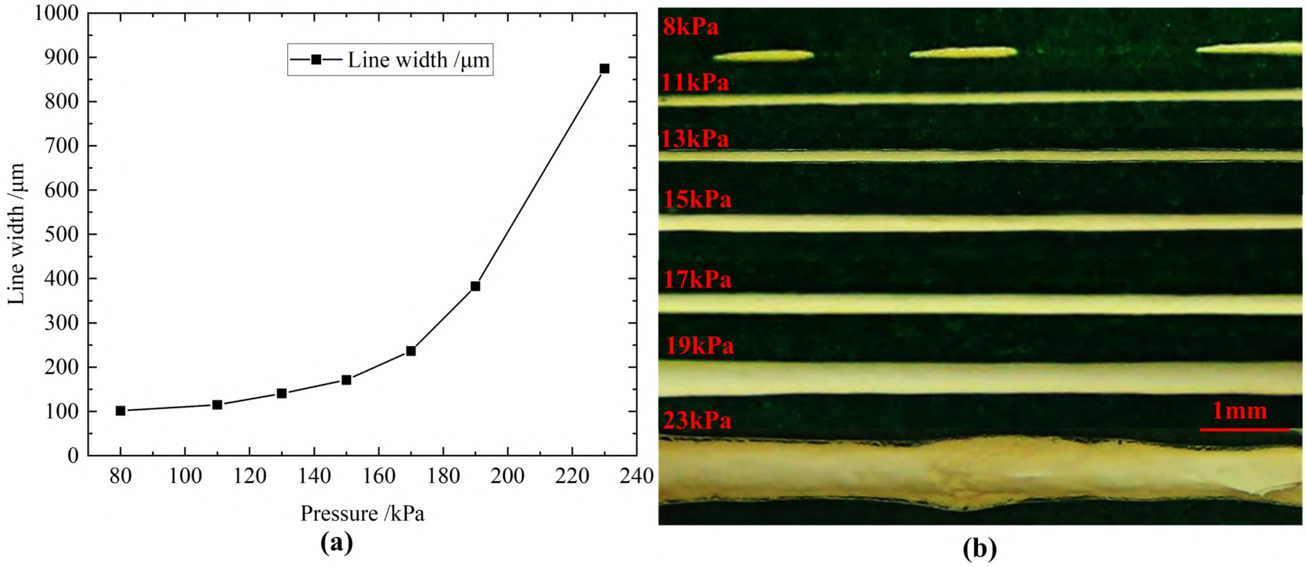

Fig. 4 Effect of the air pressure on the line width and shape of the printed silver wires: (a) line width; (b) line shape.

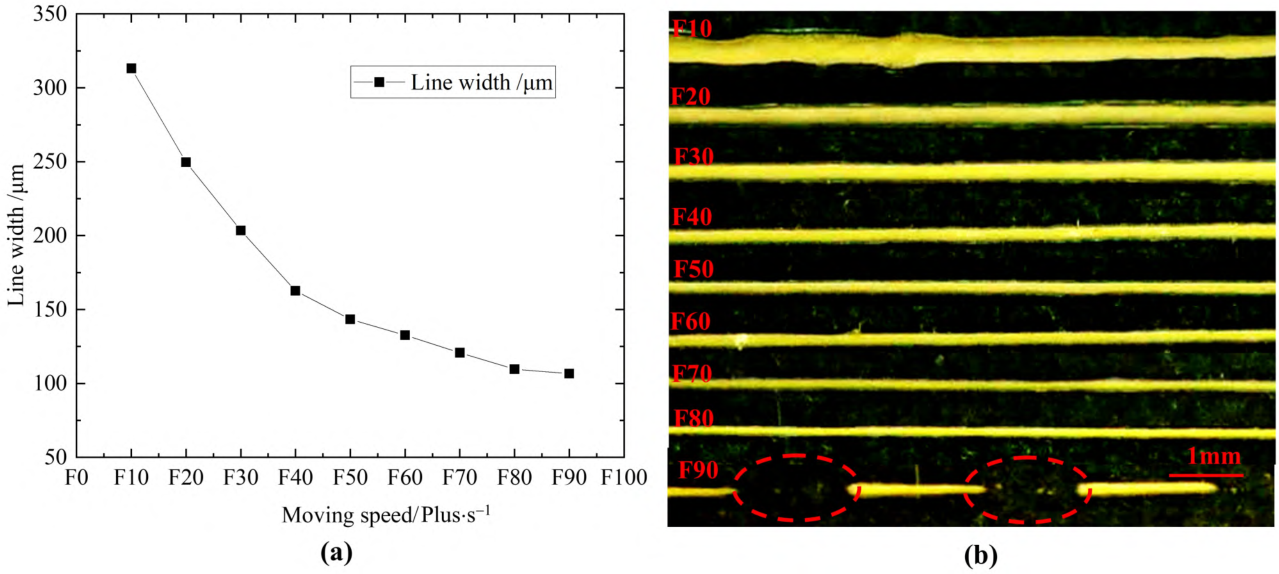

Fig. 5 Effect of the printing speed on the line width and shape of the printed silver wires: (a) line width; (b) line shape.

dimensions and morphology of the silver wires, the printing results were comprehensively analyzed under pressures of 80, 110, 130, 150, 170, 190, and 230 kPa, while maintaining the other processing parameters constant, namely a printing height of 300 μm, a DC voltage of 1300 V, a printing speed of F50, and a nozzle diameter of 300 μm.

Fig. 4(a) depicts the effect of the printing pressure on the line width of the printed silver wires. With increasing pressure, the extrusion rate of the material from the nozzle rises, resulting in a gradual broadening of the line width. Across the pressure range from 80 to 230 kPa, the measured line widths are 101.52, 114.83, 141.69, 171.24, 236.45, 382.46, and 894.36 μm, respectively. At 190 kPa, the line width exceeds the nozzle diameter. The ratio of line width to nozzle diameter ranges from a minimum of 33.8% to a maximum of 298.1%.

Fig. 4(b) illustrates morphological evolution of the printed silver wires under various printing pressures. At 80 kPa, the printing process is not continuous as indicated by clear discontinuities in the silver wire. From 110 to 190 kPa, the silver wires become continuous and uniform, with a constant increase in line width. However, at 230 kPa, both the line width and the wire thickness become irregular, and the edge roughness increases significantly, with the line width far exceeding the nozzle diameter.

These trends are attributed to the interplay between the material supply rate and the printing speed. At 80 kPa, the supply rate is insufficient for the set printing speed (F50), resulting in unstable and discontinuous material delivery. Between 110 and 190 kPa, the supply rate is optimal for the set printing speed, but the contribution of the electric field force is reduced relative to that of the pressure-driven force. This transition shifts the extrusion mechanism from electric field-induced "pulling" to pressure-driven "pushing", leading to a progression from narrower, electrically drawn wires to wider, pressure-extruded wires. At 190 kPa, the electric field force becomes negligible, causing the line width to exceed the nozzle diameter. As the pressure reaches 230 kPa, the supply rate is excessive for the set printing speed, leading to material accumulation and rapid ejection at the nozzle. This results in deformed, unevenly distributed silver wires with non-uniform thickness, density, and significantly increased roughness.

(3) Effect of the Printing Speed

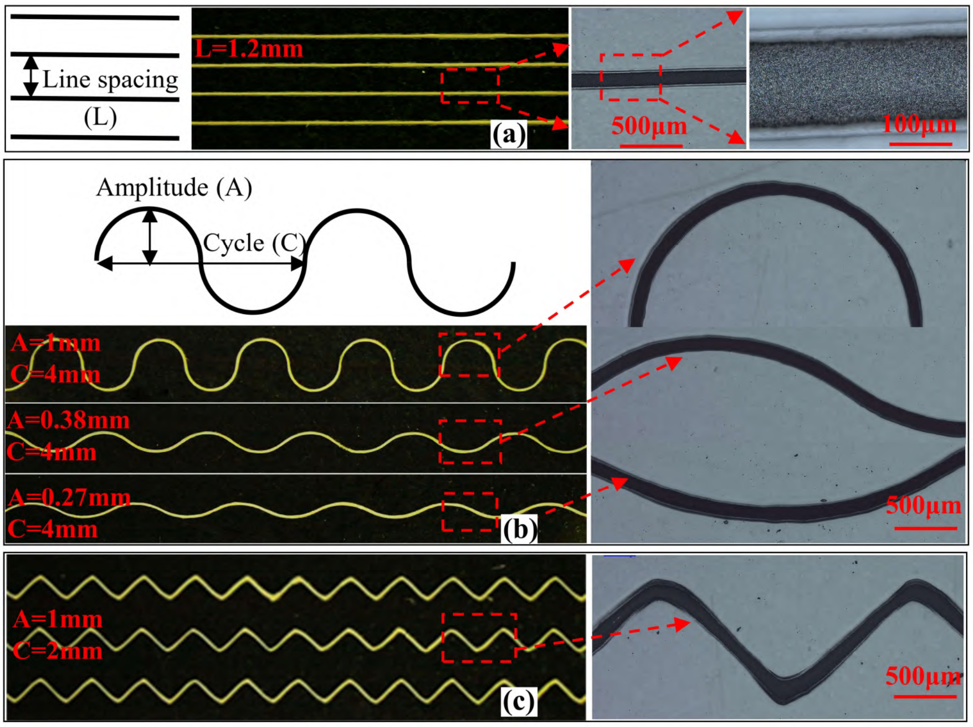

Fig. 6 Different linear patterns: (a) Grid structure; (b) Wave structure; (c) Zigzag structure

Printing speed refers to the movement speed of the printhead relative to the printing platform. When printing high-viscosity, high-silver-content nanoparticle ink on PET substrates via electric field-driven jet printing, the "necking effect" of the Taylor cone aids in achieving finer line widths. Furthermore, increase in the printing speed enables the working platform to stretch the ink further, which results in thinner lines. Therefore, printing speed is a critical parameter in controlling the line width. In this experiment, the printing speed was varied from F10 to F90, while maintaining the other processing parameters constant, namely a voltage of 1300 V, a pressure of 130 kPa, a printing height of 300 µm, and a nozzle diameter of 300 µm.

Figure 5(a) illustrates how printing speed affects the width of the printed silver wires. The findings indicate an inverse relationship between printing speed and line width, with higher speeds resulting in narrower lines. At the lowest printing speed (F10), the line width is the widest (313.17 µm), slightly exceeding the nozzle diameter. By contrast, at the highest printing speed (F90), the line width is reduced to 106.59 µm, which corresponds to a minimum line width-to-nozzle-diameter ratio of 35.53%. The measured line width differences between successive increases in printing speed are 63.52, 46.18, 40.79, 20.34, 9.72, 11.81, 11.18, and 3.04 µm, respectively. These findings indicate that the impact of the printing speed on the line width is more pronounced at lower speeds (F10–F40), while at higher speeds, the reduction becomes less substantial. This behavior is attributed to the drag force exerted on high-viscosity silver ink, which increases with the printing speed, rapidly reducing the line width. Beyond a printing speed of F50, the drag force approaches the surface tension limit of the ink, causing further increase in speed to have a negligible effect on the line width.

Fig. 5(b) illustrates the microscopic morphology of the silver wires printed at various printing speeds. At a printing speed of F10, a poor line uniformity and high edge roughness are observed due to the fact that the printing speed is insufficient for the set material supply rate. This mismatch results in accumulation of ink at the nozzle and consequent uneven deposition, compromising the wire uniformity and smoothness. At printing speeds between F20 and F70, line uniformity and edge smoothness improve as the printing speed is suitable for the set supply rate, ensuring stable and continuous ink delivery. Higher speeds also stretch the deposited ink, thus reducing the line width. However, a printing speed of F80 is too high for the set supply rate, which leads to localized material accumulation or insufficient deposition, disrupting wire uniformity. Finally, at a printing speed of F90, the imbalance becomes severe, with the nozzle moving too quickly for adequate material deposition, ultimately causing wire breakage.

C. Printing of Different Line Patterns

Grid structures with simple geometries and adjustable parameters (e.g., line width and spacing) are widely employed in numerous applications, such as transparent conductive electrodes for touch screens, solar cell electrodes, and strain and pressure sensors. Stretchable designs (e.g., wavy or zigzag patterns) alleviate strain on nanowires under mechanical stress, thereby reducing the likelihood of fracture and enhancing the stretchability of the conductive film. Herein, PET substrates were successfully patterned with grid structures, wavy lines, and zigzag designs, achieving a line width of approximately 142 µm, as illustrated in Fig. 6. The fabrication process was conducted using a voltage of 1.3 kV, a pressure of 130 kPa, a printing height of 300 µm, a nozzle diameter of 300 µm, and a printing speed set to F50.

Fig. 6(a) illustrates a grid structure exhibiting high regularity with precise and regular line spacing of 1.2 mm. The line morphology is uniform, continuous, and smooth, devoid of noticeable undulations, discontinuities, or variations in width. These characteristics reflect the excellent

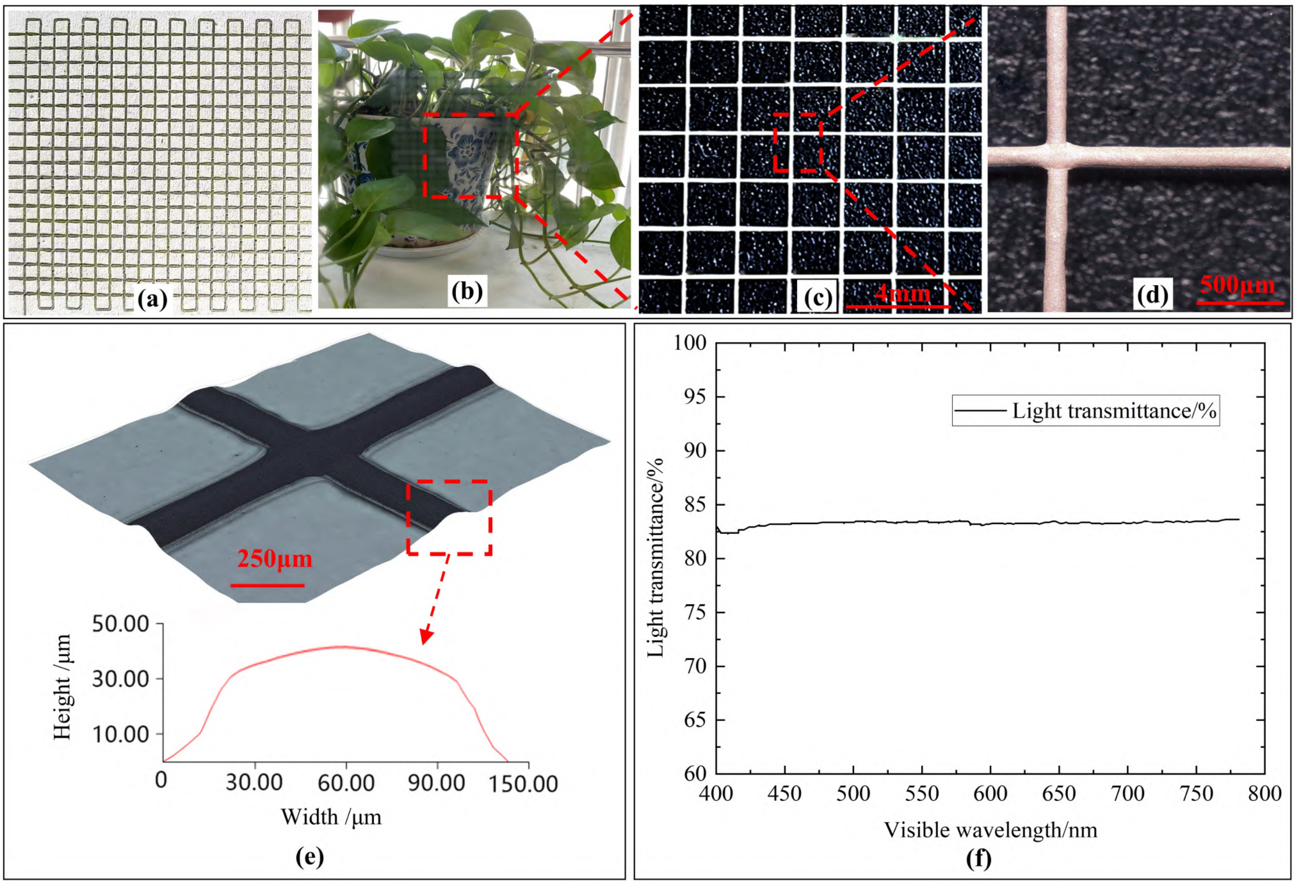

Fig. 7 Transparent conductive films: (a) macroscopic light transmission; (b), (c) microscopic images; (d) 3D morphology; (e) transmittance.

geometric uniformity and surface smoothness of the printed grid.

Fig. 6(b) displays three wavy structures with a period of 4 mm and amplitudes of 1, 0.38, and 0.27 mm, respectively. These wavy patterns exhibit precise periodic oscillations and maintain high uniformity and stability at different amplitudes. The curves remain uniformly smooth, with no abrupt changes, depressions, or protrusions, and the curvature transitions are continuous and uniform.

Fig. 6(c) shows a zigzag structure with an amplitude of 1 mm and a period of 2 mm. Although the structure is generally uniform, a slight line thickening occurs at the corner regions. This is due to the narrow spacing between the adjacent straight segments at the corners, causing silver ink to merge and overlap during printing. This overlap disrupts the uniform line width distribution and results in localized material accumulation.

D. Fabrication of Silver Mesh Transparent Conductive Films

Based on the abovementioned findings, square silver grids were printed onto a 1-mm-thick flexible transparent PET substrate that had been previously ultrasonically cleaned. The printed grids were then sintered in a vacuum furnace at 120 °C for 30 min. The resulting transparent silver grid film, shown in Fig. 7, acquired the following dimensions: line width of 142 μm, period of 2000 μm, and patterned area of 40 × 40 mm^2. The key printing parameters for the metal grid were a pressure of 130 kPa, a printing speed of F50, a printing height of 0.3 mm, and a nozzle diameter of 300 μm. Fig. 7(a) shows the macroscopic overall morphology of the electrode. Fig. 7(b) exhibits good transparency of the flexible electrode. Fig. 7(c) and (d) display the microstructure at different magnifications, revealing smooth edges in the silver wire pattern with no burrs and continuous silver lines, which demonstrates a high pattern uniformity. Fig. 7(e) illustrates the 3D morphology of the grid, with the deposition height of a single silver line being approximately 39 μm and the height-to-width ratio being about 0.27.

The performance of transparent conductive films is primarily assessed using two parameters; namely, transmittance (T) and sheet resistance (Rs). For square-patterned silver meshes, the transmittance can be theoretically calculated by using the following equation [24]:

$$T = 1 - \frac{P \times W + (P - W) \times W}{P^2}, \tag{1}$$

where W is the width of the silver line and P denotes the period of the silver mesh. Optical transmittance is generally evaluated at a wavelength of 550 nm. In this study, a UV–visible spectrophotometer (UV-6100) was utilized to assess the transmittance of the samples, offering a wavelength accuracy of ±0.3 nm and a repeatability of ±0.1 nm. Fig. 7(f) presents that the transmittance at 550 nm was found to be 83.36%.

The sheet resistance was measured using a DC resistance tester (AT156), with an accuracy of 0.05% and a sampling rate of 140 times per second (7 ms per measurement). The measured sheet resistance was 2.08 Ω·sq^{-1}. To evaluate the balance between the optical and electrical performance of optoelectronic devices, the figure of merit (*FoM*) is commonly used. The *FoM* can be calculated by the method proposed by Dressel and Gruner as follows [25]:

$$FoM = \frac{188.5}{R_S(T_{550nm}{}^{-1/2} - 1)}, \quad (2)$$

where $T_{550nm}{}^{-1/2}$ is the transmittance at a wavelength of 550 nm. A higher *FoM* value indicates a superior optoelectronic performance. By substituting the measured values into the abovementioned equation, the *FoM* of the flexible transparent conductive film prepared in this study was calculated to be 951. This high *FoM* demonstrates that the film exhibits a relatively low sheet resistance and a high transmittance, significantly better than those of traditional ITO, which typically has a *FoM* of around 300 [26]. Therefore, the flexible transparent conductive film developed in this study presents a promising solution for large-scale, low-cost industrial production.

IV. CONCLUSION

This research introduces an innovative technique for producing flexible, transparent conductive films with metal-grid patterns using electric field-driven jet printing. The proposed approach overcomes the limitations of conventional printing techniques, which are constrained by the nozzle diameter, and thus cannot be used to print patterns with line widths smaller than the nozzle diameter. Moreover, conventional approaches struggle with printing nano-silver inks that have both high viscosity and a high silver content. Experimental findings confirm that this technique facilitates the even deposition of such inks onto diverse non-conductive surfaces. The printed wire widths are significantly smaller than the nozzle diameter by an order of magnitude, while also demonstrating remarkable consistency and adaptability, thereby verifying the effectiveness of this approach. With optimized parameters, a 40 × 40-mm^2 metal-grid transparent conductive film was successfully printed. The film displays a uniform line morphology, high optical transmittance (83.36%), low sheet resistance (2.08 $\Omega\cdot sq^{-1}$), and high *FoM* (951), highlighting the promising potential of the developed technology for flexible electronics applications.

REFERENCES

[1] Xiuhuai Jia, Pan Yang, Le Zhao, Dawei Du, and Zilan Wang, "Ultrathin Ag@ ZnO Core–Shell nanowires for stable flexible transparent conductive films,". ACS Applied Electronic Materials, vol. 5, no.8, pp4198-4208, 2023.

[2] Zhijiang Guo, Xiaoli Li, Ning Li, Xuanji Liu, and Haojie Li, "Multilayer directionally arranged silver nanowire networks for flexible transparent conductive films," Physical Chemistry Chemical Physics, vol. 25, no.21, pp14778-14785, 2023.

[3] Velarde-Gomez, Sergio, Alexander Molina-Cabrera, and Eduardo Giraldo, "Model-based Adaptive Control of a 3D Printed Permanent Magnet Synchronous Motor," Engineering Letters, vol. 31, no.4, pp1804-1812, 2023.

[4] Fulai Cao, Yanpu Chao, Shuai Lu, Ruirui Guo, and Yaohui Li, "Electric Field-driven Fused Deposition of High-resolution Polycaprolactone Microstructures," Engineering Letters, vol. 32, no.7, pp 1385-1393, 2024.

[5] Domanski, and Zbigniew, "Damage Statistics in Progressively Compressed Arrays of Nano-pillars," Engineering Letters, vol. 27, no.1, pp18-23, 2019.

[6] Xinyi Zeng, Yanqing Tang, Xiaoyi Ca, Jianxin Tang, and Yanqing Li, "Solution-processed OLEDs for printing displays," Materials Chemistry Frontiers, vol. 7, no.7, pp 1166-1196, 2023.

[7] Karthikeyan Vijayan, S.P. Vijayachamundeeswari, Kalainathan Sivaperuman, Nazmul Ahsan, and Thirumalaisamy Logu, "A review on advancements, challenges, and prospective of copper and non-copper based thin-film solar cells using facile spray pyrolysis technique," Solar Energy, vol. 234, no.1, pp 81-102, 2022.

[8] Edzer Huitema, and Ian French, "E Ink's Technicolor Moment: The Road to Color E-Paper Took Two Decades," IEEE Spectrum, vol. 59, no.2, pp 30-35, 2022.

[9] Uday Shankar, Deepa Oberoi, and Anasuya Bandyopadhyay, "A review on the alternative of indium tin oxide coated glass substrate in flexible and bendable organic optoelectronic device," Polymers for Advanced Technologies, vol. 33, no.10, pp 3078-3111, 2022.

[10] Li Liu, Jianchun Jiang, Zhan Xu, Jiahang Zhou, and Yunbo Li, "Enhanced electrical conductivity of PEDOT-encapsulated silver nanowire film pretreated with surfactants," Colloid and Polymer Science, vol. 299, no.1, pp 595-601, 2021.

[11] Jiazhen Sun, Rui Sun, Peng Jia, Mengdi Maa, and Yanlin Song, "Fabricating flexible conductive structures by printing techniques and printable conductive materials," Journal of Materials Chemistry C, vol. 10, no.25, pp 9441-9464, 2022.

[12] Evgeny Senokos, Moumita Rana, Maria Vila, Julio Fernandez-Cestau, and Rubén D. Costa, "Transparent and flexible high-power supercapacitors based on carbon nanotube fibre aerogels," Nanoscale, vol. 12, no.32, pp 16980-16986, 2020.

[13] Yanmin Wang, Aiping Liu, Yongqin Han,and Tingxi Li, "Sensors based on conductive polymers and their composites: a review," Polymer International, vol. 69, no.1, pp 7-17, 2020.

[14] Zahra Fakharan,and Ali Dabirian, "Metal grid technologies for flexible transparent conductors in large-area optoelectronics," Current Applied Physics, vol. 31, no.1, pp 105-121, 2021.

[15] Silvia Varagnolo, Keun-Woo Park, Jin-Kyun Lee, and Ross A. Hatton, "Embedded-grid silver transparent electrodes fabricated by selective metal condensation," Journal of Materials Chemistry C, vol. 8, no.38, pp 13453-13457, 2020.

[16] Philip Bellchambers, Silvia Varagnolo, Corinne Maltby, and Ross A. Hatton, "High-performance transparent copper grid electrodes fabricated by microcontact lithography for organic photovoltaics," ACS Applied Energy Materials, vol. 4, no.4, pp 4150-4155, 2021.

[17] Lukas F. Engel, Lola González-García ORCID, and Tobias Kraus, "Flexible and transparent electrodes imprinted from metal nanostructures: morphology and opto-electronic performance," Nanoscale Advances, vol. 4, no.16, pp 3370-3380, 2022.

[18] Yilun Wang, Shuangshuang Li, Baojia Li, Yao Zhang, and Lijing Huang, "Ultrafast laser direct writing on PVP/FTO/Glass substrates to fabricate Ag mesh transparent conductive films," Ceramics International, vol. 47, no.10, pp 14087-14096, 2021.

[19] Zhi Wang, Guangming Zhang, Hui Huang, Lei Qian, and Xiaoling Liu, "The self-induced electric-field-driven jet printing for fabricating ultrafine silver grid transparent electrode," Virtual and Physical Prototyping, vol. 16, no.1, pp 113-123, 2021.

[20] Guangming Zhang, Hongbo Lan, Lei Qian, Jiawei Zhao, and Fei Wang, "A microscale 3D printing based on the electric-field-driven jet," 3D Printing and Additive Manufacturing, vol. 7, no.1, pp 37-44, 2020.

[21] Zhifeng Han, Guangming Zhang, Yirui Li, Kai Shi, and Lingxuan Ma, "High resolution conformal additive manufacturing based on electric-field-driven jet 3-axis micro-3D printing," Journal of Manufacturing Processes, vol. 127, no.1, pp 35-42, 2024.

[22] Wenzheng Sun, Zhenghao Li, Xiaoyang Zhu, Houchao Zhang, and Hongke Li, "Electric Field-Driven Jetting and Water-Assisted Transfer Printing for High-Resolution Electronics on Complex Curved Surfaces," Electronics, vol. 13, no.7, pp 1-14, 2024.

[23] Fulai Cao, Yanpu Chao, Hao Yi, Shuai Lu, and Chengshui Guo, "Design and Experimental Testing of an Electric Field-Driven Droplet Injection Device," Fluid Dynamics & Materials Processing, vol. 19, no.11, pp 1-15, 2023.

[24] Bin Zhang, Hyungdong Lee, and Doyoung Byun, "Electrohydrodynamic jet printed 3D metallic grid: toward high-performance transparent electrodes," Advanced Engineering Materials, vol. 22, no.5, pp 1-10, 2020.

[25] Dressel, Martin, and George Grüner, *Electrodynamics of solids: optical properties of electrons in matter*. Cambridge university press, 2002, ch. 6.

[26] Ryoko Suzuki, Yasutaka Nishi, Masaki Matsubara, Atsushi Muramatsu, and Kiyoshi Kanie, "Suzuki R, Nishi Y, Matsubara M, et al. A nanoparticle-mist deposition method: Fabrication of high-performance ITO flexible thin films under atmospheric conditions," Scientific Reports, vol. 11, no.1, pp10584, 2021.